PCCP

RSC Publishing

PAPER

View Article Online
View Journal | View Issue

Cite this: *Phys. Chem. Chem. Phys.*, 2013, **15**, 6049

Liquid state DNP of water at 9.2 T: an experimental access to saturation†

Petr Neugebauer,[a] Jan G. Krummenacker,[a] Vasyl P. Denysenkov,[a] Giacomo Parigi,[bc] Claudio Luchinat[bc] and Thomas F. Prisner*[a]

Received 11th December 2012,
Accepted 15th February 2013

DOI: 10.1039/c3cp44461a

www.rsc.org/pccp

We have performed liquid state (''Overhauser'') Dynamic Nuclear Polarization (DNP) experiments at high magnetic field (9.2 T, corresponding to 260 GHz EPR and 400 MHz ^{1}H-NMR resonance frequency) on aqueous solutions of ^{14}N-TEMPOL nitroxide radicals. Integrated signal enhancements exceeding −80 were observed for the water protons at microwave superheated temperatures (160 °C) and still −14 at ambient temperatures (45 °C) relevant to biological applications. Different contributions contributing to the DNP enhancement such as saturation factor, leakage factor and sample temperature under microwave irradiation could be determined independently for a high spin concentration of 1 M, allowing the calculation of the coupling factors as a function of temperature and a quantitative comparison of this parameter with values derived from field dependent relaxation measurements or predictions from MD simulation.

Introduction

Improving sensitivity is a key issue in Nuclear Magnetic Resonance (NMR) spectroscopy. Even a small signal enhancement by a factor of 2 shortens the acquisition time by a factor of 4. One way of tackling the sensitivity issue is hyperpolarization by Dynamic Nuclear Polarization (DNP). In DNP, hyperpolarization of nuclei is achieved by microwave (MW) irradiation of the unpaired electron spin of radicals (polarizing agents), which are part of the sample under study, to transfer their larger Boltzmann polarization to the nuclei.[1–3] At high magnetic fields, pioneering work has been performed in the solid state,[4,5] leading to a surge of new developments and applications.[6–9] More recently, high field DNP in the liquid state has become a field of study, with new developments at *e.g.* 3.4 T[10–13] and 9.2 T.[14–17] In the liquid state, the active DNP mechanism is the Overhauser effect.

The Overhauser enhancement can be written as

$$\varepsilon_{OE} = \frac{\langle I_z \rangle - I_0}{I_0} = \frac{\gamma_e}{\gamma_n} \cdot f \cdot s \cdot \xi \qquad (1)$$

where γ_e and γ_n are the gyromagnetic ratios of the electron and the nucleus, respectively, *i.e.* $\gamma_e/\gamma_n \approx -660$ for protons,[18] $f = 1 - T_{1R}/T_{1W}$ is the leakage factor, which can be determined from the nuclear T_1 in the presence (T_{1R}) and in the absence of radicals in the solution (T_{1W}), and reflects the influence of radicals on the nuclear relaxation rate of the used solvent. The factor s denotes the saturation factor, which describes how well the electron transition is saturated by the MW irradiation. It ranges from 0 for no saturation, *i.e.* thermal population, to 1 for a fully saturated electron spin transition with equalized populations. The last parameter is called the coupling factor ξ. While the optimization of f and s is rather a technical issue, the coupling factor reflects the nature of the polarization transfer between the electron and nuclear spins and cannot be easily controlled. If the magnetic dipole–dipole coupling is the dominant mechanism, as usually the case for protons of target molecules in liquids, the coupling factor ranges between 0 and 0.5. This yields a maximal theoretical enhancement ($\xi = 0.5$, $s = 1$, $f = 1$) of −330. The coupling factor and its temperature dependence were independently determined from the field dependence of the solvent water proton relaxivity (also called Nuclear Magnetic Relaxation Dispersion – NMRD) profiles[12,19–22] and compared with the values obtained using DNP.

Experimental

DNP measurements

The DNP experiments were performed on a setup, which consists of a commercial 400 MHz NMR spectrometer (Bruker Avance),

[a] *Institute of Physical and Theoretical Chemistry and Center for Biomolecular Magnetic Resonance, Goethe-University, Max-von-Laue-Str. 7, 60438, Frankfurt am Main, Germany. E-mail: prisner@chemie.uni-frankfurt.de*
[b] *Department of Chemistry, University of Florence, via della Lastruccia 3, 50019, Sesto Fiorentino, FI, Italy*
[c] *CERM, University of Florence, Via Luigi Sacconi 6, 50019, Sesto Fiorentino, FI, Italy*

† Electronic supplementary information (ESI) available. See DOI: 10.1039/c3cp44461a

equipped with a home built MW bridge operating at 260 GHz for Electron Paramagnetic Resonance (EPR) excitation, and a home built double resonance DNP probe (260 GHz/400 MHz).[23]

The DNP probe consists of a helix coil for NMR excitation and detection made of a copper tape, which serves as the body of a TE_{011} cylindrical resonator for the EPR excitation at the same time (double resonance structure), as depicted in Fig. 1. The probe further contains a Radio Frequency (RF) tuning setup and the metal–dielectric MW waveguide (Institute of Radiophysics and Electronics – IRE, Ukraine) to propagate the MW. The leads of the helix coil are connected to the RF circuit tuned to 400 MHz NMR frequency. The MW resonance mode is maintained inside of the helix coil between two plungers made of MACOR (Corning Inc.) with silver coated caps. This MW resonance structure is coupled to the MW waveguide in the middle of the helix coil through an elliptical iris (0.4 mm by 0.25 mm). For MW cavity tuning, one of the plungers can be moved from the outside of the probe *via* gears and a driving rod. The RF of the NMR circuit can be tuned in the range from 390 to 400 MHz; its conversion factor is 0.17 mT $W^{-1/2}$ and its quality factor Q_{RF} is about 70. The MW resonance of the cavity can be tuned between 256 and 260 GHz, typically reaching a conversion factor of 0.45 mT $W^{-1/2}$ and a quality factor Q_{MW} of approximately 400.[15] The necessary MW power for a DNP experiment at 260 GHz is produced using a high power (20 W) gyrotron source (Gycom, Russia). Power transmission to the MW bridge is achieved *via* a corrugated waveguide transmission line (Gycom) with a total length of 12 m. The MW bridge consists of oversized waveguides, calibrated attenuators, a beam splitter (all IRE, Ukraine) and two zero-bias Schottky diodes (VDI-WR3ZBD-S027C, Virginia Diodes) used for incident power monitoring and cavity tuning. The total MW losses from the gyrotron to the DNP probe are approximately 4 dB. For more details concerning the DNP spectrometer see the work of Denysenkov *et al.*[15,23]

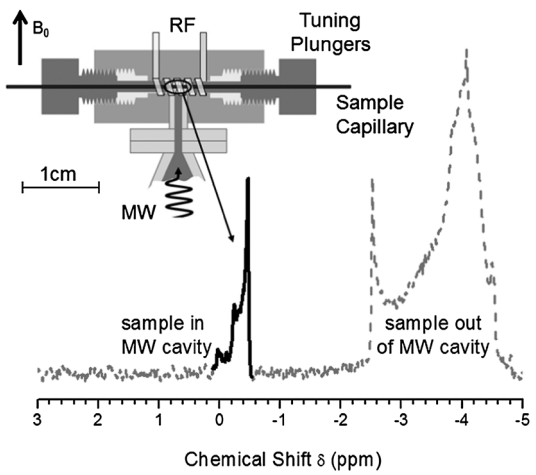

Fig. 1 Schematic drawing of the double resonance structure used for ^{1}H-NMR at 400 MHz and EPR at 260 GHz simultaneously (top left) and a typical ^{1}H-NMR spectrum of water obtained with this setup. The peak at −0.4 ppm corresponds to the sample inside of the MW cavity, while the large signal between −2.5 and −4.5 ppm is due to the sample outside of the MW cavity.

For DNP measurements the liquid sample is put into a quartz capillary (Polymicro) of 50, 30 or 20 μm inner diameter (ID) with the same 150 μm outer diameter (OD). The capillary is sealed with wax on both ends and placed along the axis of the cylindrical double resonance cavity. The size of the MW cavity is approximately 1.6 mm, which leads to effective sample volumes of 3, 1.1 or 0.5 nl for 50, 30 or 20 μm ID capillaries, respectively.

For typical NMR experiments not requiring a double resonance structure, such as T_{1n} measurements, a commercial 400 MHz liquid state probehead was used (Bruker BBI).

Both probeheads can be equipped with a temperature control unit (BCU 05, Bruker), bringing the sample to a set temperature using a stream of gas.

The DNP enhancements were determined by taking the ^{1}H FT-NMR spectra of the samples in the MW cavity (Fig. 1) with and without continuous wave (CW) MW irradiation of the (central) hyperfine line of the ^{14}N-TEMPOL nitroxide radicals, respectively. The proton NMR lines are then integrated to determine the signal strength, while the integrated enhancement is calculated using eqn (1).

CW-EPR measurements were performed with our home built pulsed high field EPR spectrometer operating at 180 GHz.[24] For measurements at temperatures higher than 25 °C an additional resistive heater was used. The sample temperature was monitored using a platinum thermometer attached to the body of the MW cavity.

NMRD measurements

Longitudinal relaxation rates at magnetic fields ranging from 0.01 to 40 MHz proton Larmor frequency were measured using the field cycling technique with a high sensitivity Stelar Spinmaster FFC-2000-1T. Errors in the measurement of the relaxation rates are below 1%. Proton relaxivity is calculated by subtracting the relaxation rates of the buffer from the relaxation rate of the ^{14}N-TEMPOL solution, and normalizing to the radical concentration. High frequency relaxation rates at 250, 400, 500 and 950 MHz were measured on corresponding NMR spectrometers.

The paramagnetic enhancement of the solvent nuclear relaxation rate is described using the inner-sphere and the outer-sphere models,[19,20,25,26] which take into account the contributions to relaxation from the dipole–dipole coupled electron and nuclear spins when positioned at a fixed distance r (R_1^{inner}) or when the nucleus in the solvent molecules is freely diffusing around the paramagnetic molecule, down to a distance of closest approach, d (R_1^{outer}), respectively.

In the inner-sphere model, if the solvent nucleus exchanges between a position where it is bound to the paramagnetic molecule and a position where it is free in solution on a time scale shorter than its relaxation time in the bound position (fast exchange regime), the paramagnetic contribution to relaxation is given by[25,26]

$$R_1^{inner} = k(7J(\omega_s,\tau_c) + 3J(\omega_I,\tau_c))$$

where

$$k = f_M \frac{2}{15}\left(\frac{\mu_0}{4\pi}\right)^2 \frac{\gamma_I^2 g_e^2 \mu_B^2 S(S+1)}{r^6},$$

$J(\omega,\tau)$ is the Lorentzian spectral density functions in the form of

$$J(\omega,\tau) = \frac{\tau}{1+\omega^2\tau^2},$$

where τ_c is the correlation time for the dipolar interaction, f_M is the mole fraction of ligand nuclei in bound positions (equal to $2 \times 10^{-3}/111$ assuming one water molecule bound to each paramagnetic molecule), ω_I and ω_s are the proton and electron Larmor frequencies multiplied by 2π, respectively, S is the electron spin quantum number, γ_I is the proton gyromagnetic ratio, μ_B is the electron Bohr magneton, g_e is the electron g factor, and μ_0 is the permeability of vacuum.

In the outer-sphere model, the translational diffusion of the ligand molecules causes a paramagnetic contribution to relaxation given by[20]

$$R_1^{outer} = k'(7\tilde{J}(\omega_s,\tau_D) + 3\tilde{J}(\omega_I,\tau_D))$$

where

$$k' = \frac{32\,000\pi}{405}\left(\frac{\mu_0}{4\pi}\right)^2 \frac{N_A[M]\gamma_I^2 g_e^2 \mu_B^2 S(S+1)}{dD},$$

$$\tilde{J}(\omega,\tau) = \frac{1+5z/8+z^2/8}{1+z+z^2/2+z^3/6+4z^4/81+z^5/81+z^6/648},$$

$z = (2\omega\tau_D)^{0.5}$, N_A is Avogadro's constant, D is the sum of the diffusion coefficients of the solvent molecule and of the paramagnetic molecule, and [M] represents the molar concentration of the paramagnetic moiety (expressed in mol dm^{-3}). This model was developed in the hypothesis of spherical molecules, with the unpaired electron in the center of the molecule. A diffusional correlation time τ_D is defined, which depends on the diffusion coefficients and on the distance of closest approach d between solvent protons and electron spins:

$$\tau_D = \frac{d^2}{D}.$$

Finally, the coupling factor results

$$\xi = \frac{5}{7}\left[1 - \frac{3kJ(\omega_I,\tau_c) + 3k'\tilde{J}(\omega_I,\tau_D)}{R_1^{inner} + R_1^{outer}}\right].$$

Results and discussion

The DNP experiments were performed over a broad range of ^{14}N-TEMPOL radical concentrations in water, ranging from 5 mM up to 1 M, and in 3 different capillary sizes.

Fig. 2 shows a DNP experiment performed on a water sample doped with 1 M of ^{14}N-TEMPOL in a 30 μm ID capillary. The irradiation MW power was approximately 600 mW, corresponding to a B_1 field of 3.5 G. The figure shows a strongly negatively enhanced signal in the MW cavity. It yields an enhancement factor of −83, the negative sign is caused by an electron–nuclear dipolar interaction typical for liquid state DNP experiments. Notably, while the signal from outside of the MW cavity remains unchanged at the same position at approximately −7 ppm, the DNP enhanced signal significantly changes its position with respect to the reference signal indicated by the arrow. This shift is caused by a combination of MW heating and the suppression of the strong paramagnetic shift of the 1 M radical concentration sample by the microwave irradiation.[27] Both contributions to the chemical shift change are important for a proper understanding of the DNP experiments and help to quantitatively analyze the parameters involved in eqn (1), which are discussed in detail in the following text.

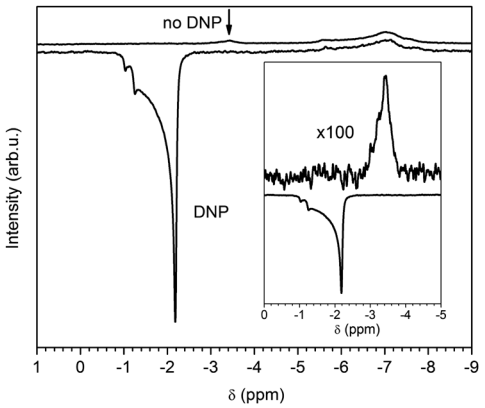

Fig. 2 Normalized ^{1}H-NMR spectra to single scan of 1 M ^{14}N-TEMPOL in water with (lower spectrum – 64 scans) and without (upper spectrum – 512 scans) MW irradiation of the sample, respectively. An integrated enhancement of −83 can be observed in the water proton signal. The inset shows the reference spectrum without irradiation enlarged by a factor of 100 for comparison.

Sample temperature calibration

The sample temperature is an important parameter involved in almost every aspect of Overhauser DNP from relaxation rates to lineshapes and molecular motion. As a consequence, for a quantitative analysis, keeping track of the sample temperature is critical. Unfortunately, the sample temperature in our DNP experiment cannot be accessed directly, *e.g.* with a thermometer. Also, accessing the sample temperature *via* the temperature dependence of the chemical shift can be problematic, because the shift is strongly dependent on the experimental configuration of the probe[28] and thus prone to error.

Therefore, we calibrated the temperature with a method similar to the use of neat ethylene glycol as a "chemical shift thermometer",[29–31] using a reference sample consisting of 90% water and 10% ethylene glycol. In this sample, the relative shift between the water proton peak and the CH_2 peak of ethylene glycol exhibits a strong temperature dependence, which was calibrated. The calibration was performed using gas heating in both the standard Bruker BBI and the DNP probeheads, yielding the same calibration curve (see ESI†). This shows that unlike the approach relying on the absolute chemical shift this approach is insensitive to experimental configurations. To obtain the sample temperature under DNP conditions at a given MW power, the DNP sample is replaced by the reference water sample containing 10% ethylene glycol, which is irradiated with the same MW power. The relative shift then provides the reference sample temperature. Assuming the dielectric losses

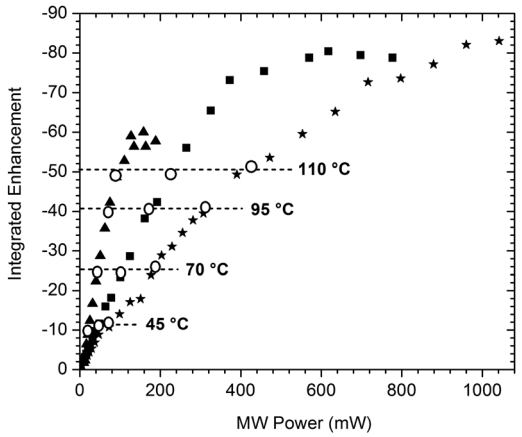

Fig. 3 The DNP enhancement plotted against the incident MW power for a 1 M ^{14}N-TEMPOL in water sample for three capillary sizes: 50 (▲), 30 (■) and 20 μm (★) ID. The temperature increase is indicated by hollow circles (○) for each capillary, dashed lines connect these points into virtual isotherms.

in water and the water–ethylene glycol mixture are the same, this temperature corresponds to the temperature of the DNP sample. To confirm this assumption the experiment was repeated using only 5% of ethylene glycol yielding the same temperature value.

Varying the sample size (capillary radius) results in varying dielectric losses in the MW resonator and thus in a variation of sample temperature for a given incident MW power. The result is shown in Fig. 3. As shown and proven by the above calibrations, the MW heating of the sample in the capillary leads to temperatures far beyond 100 °C which is well known as "superheated water",[32] before further increasing the MW power destroys the sample in the MW cavity. Furthermore, our DNP probe (*i.e.* the MW cavity) has an inhomogeneous irradiation profile over the DNP sample (see ESI†), which leads to a temperature gradient across the sample. At low irradiation power the temperature gradient is low, whereas at high irradiation power it becomes more significant.[14] However, higher sample diffusion rates can smooth the temperature gradient effect. Since we monitor NMR peak positions, the stated temperatures represent the highest temperature in the sample and should therefore be considered as lower boundaries for possible ε values.

For more details concerning the DNP sample temperature see Fig. S1 of the ESI.†

Leakage factor *f*

The leakage factor, which reflects the introduction of a strong relaxation pathway by adding radicals to the solution was measured for all mentioned radical concentrations and in a broad temperature range from room temperature, *i.e.* 25 °C to 95 °C, *i.e.* just below the boiling point of water. An excerpt of this is displayed in Table 1.

Being in the extreme narrowing limit, T_1 becomes longer with increasing temperature. Typically, nuclear T_1 of water spans values from 3 s to 10 s in a temperature range from 25 °C to 95 °C. However, the strongly temperature dependent effects on T_1 in the presence and in the absence of radicals almost cancel out completely in the ratio, so the leakage factor turns out to be almost independent of the temperature of our experiment. Because adding radicals to the solution adds a strong relaxation pathway and thus shortens nuclear T_1, the leakage factor shows a monotonic increase with radical concentration. Already at 40 mM ^{14}N-TEMPOL concentration, the leakage factor has reached 0.95 and at 200 mM it is 0.99 and therefore practically at its theoretical maximum of 1.

Table 1 Measured leakage factor *f* as a function of ^{14}N-TEMPOL concentration and the sample temperature

	200 mM	100 mM	40 mM	20 mM	5 mM
25 °C	0.99	0.98	0.95	0.90	0.66
95 °C	0.99	0.98	0.94	0.89	0.64

The concentration dependence of the leakage factor therefore dominates the fast rise of the observed DNP enhancements up to 100 mM (Fig. 4). A further increase in the enhancement can be attributed to Heisenberg (spin) exchange, collapsing the three EPR lines of ^{14}N-TEMPOL into a single line at high concentration (Fig. 5), making saturation easier. The spread of the DNP enhancements for a given isotherm in Fig. 4 is due to the capillary change between consecutive measurements, which leads to slightly different MW couplings and thus sample temperatures.

Saturation factor *s*

The saturation factor *s* in a DNP experiment is in general hard to access experimentally, especially at high magnetic fields, by EPR methods, as for example ELDOR,[33] due to very short electron spin relaxation times T_{1e} and T_{2e} of nitroxide radicals in liquid solution. Also, extrapolating the experimentally observed DNP enhancements to full saturation by a power curve[18] will not work well as the MW irradiation of the sample always results in a change of the sample temperature. Since the extrapolation to infinite MW power is unstable in the first place, the temperature deviation prevents the power curve method from giving a result with a reasonable error.

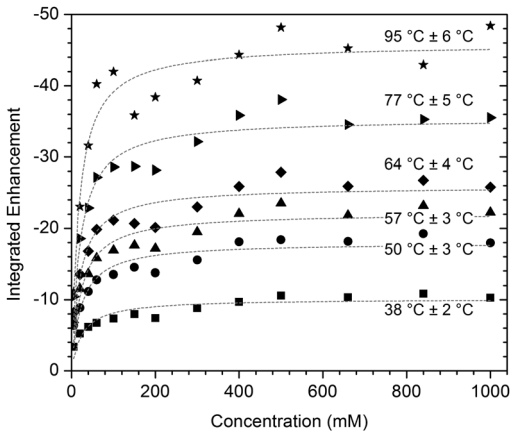

Fig. 4 Dependence of the integrated DNP enhancement on the ^{14}N-TEMPOL concentration for various irradiation powers and hence sample temperatures, as indicated in the figure. The experiment was performed using 30 μm ID capillaries.

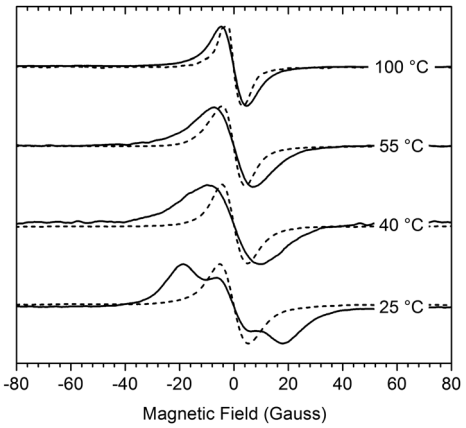

Fig. 5 180 GHz CW-EPR spectra of ^{14}N-TEMPOL in water samples with 100 mM (solid lines) and 1 M (dotted lines) radical concentration, respectively, at various temperatures ranging from room temperature (bottom) to the boiling point (top). In this regime both elevated temperature and radical concentration narrow the EPR line, making saturation easier.

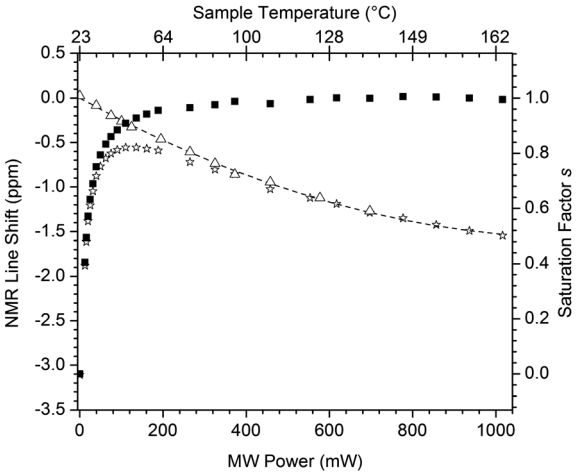

Fig. 6 NMR line shifts of the peak of a pure water sample (△) and a 1 M ^{14}N-TEMPOL in water sample (☆), plotted against the incident MW power. Through the microwave heating calibration each irradiation power can be assigned a sample temperature (temperature scale on top). By subtracting the temperature shift from the total NMR shift the pure paramagnetic shift is obtained, which can be scaled to yield the saturation factor (■, scale on the right).

Consequently, we explored a method where s is accessed *via* the paramagnetic shift. This idea to determine the saturation of the EPR line has been already presented in the work of Wind *et al.*[34] reducing the Knight shift in a fluoranthenyl radial anion salt one-dimensional crystal, and by Gafurov *et al.* for DNP measurements in aqueous solutions of Fremy's salt.[14] In a DNP sample in a static magnetic field, the nuclei experience a certain paramagnetic shift, depending on the radical concentration and on the interaction of the radicals with the solvent.[27] If the electron spin transition is now saturated, the electron spin polarization is diminished. In consequence, the paramagnetic shift is diminished as well. At full saturation, *i.e.* equalized electron spin populations and no polarization left, the paramagnetic shift has disappeared altogether. If the temperature effect on the chemical shift and the variation of the paramagnetic shift can be distinguished well, monitoring the NMR peak position gives a direct access to s. By subtracting the temperature dependent chemical shift of a reference sample without radicals from the total NMR shift of the DNP sample the pure paramagnetic shift is obtained. This allows determining the saturation factor s.

Because the paramagnetic shift scales linearly with the radical concentration, high concentrations are required to apply this method. For a sample with 1 M concentration of ^{14}N-TEMPOL in water the paramagnetic shift is large enough to do so, as can be seen in Fig. 6.

Fig. 6 shows that for a 20 μm ID capillary a MW power of roughly 100 mW is sufficient to achieve >0.9 saturation. For MW powers above 200 mW the saturation factor s does not improve anymore, but the sample is heated further. As a consequence, the NMR line shift of the DNP sample follows the temperature shift of the pure water.

The dependence of the saturation factor s on the applied MW power can be better understood from the CW-EPR spectra of the DNP samples. The narrower the EPR linewidth of the respective spectrum, the easier it is to saturate the corresponding EPR transition. The EPR spectrum is determined by the radical concentration and by the temperature through the MW heating during the DNP experiment. As can be seen in Fig. 5, both an elevated temperature and a higher concentration make the Heisenberg (spin) exchange rate higher, which causes the three hyperfine lines of ^{14}N-TEMPOL to collapse into one. For the 1 M sample the spin exchange rate at 25 °C is large enough, so the temperature effect on the linewidth is less pronounced than in the case of the 100 mM sample. This linewidth dependence on radical concentration and temperature also affects the DNP enhancement for low concentration samples (Fig. 4).

Coupling factor ξ from NMRD

The relaxation profiles of a 40 mM TEMPOL solution were acquired from 25 °C to 80 °C, and normalized to 1 mM radical concentration after subtraction of the pure water relaxation rates. The profiles, reported in Fig. 7, show that relaxivity is almost constant at low fields and then decreases (according to the spectral density functions previously reported) to approach the smaller high field values, when the $J(\omega_s,\tau_c)$ and $\tilde{J}(\omega_s,\tau_D)$ terms approach zero. This decrease in relaxivity is called dispersion. The dispersion is centred at the proton Larmor frequency with a relaxivity value equal to the average between the low field value and the high field value with the $J(\omega_s,\tau_c)$ and $\tilde{J}(\omega_s,\tau_D)$ terms approaching zero. Fig. 7 shows that the centre of the dispersion for the profiles acquired at different temperatures is positioned at higher fields with increasing temperature. This is a clear indication of the expected decrease with temperature of the correlation time of the motions modulating the water proton–unpaired electron hyperfine interaction.[26] In turn, this indicates that the coupling factor increases with temperature, as expected.[19] The profiles were fitted according to the outer-sphere and inner-sphere relaxation models, *i.e.*, as

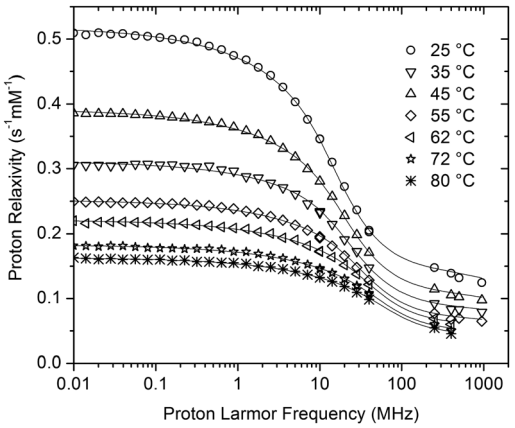

Fig. 7 Solvent water ^{1}H relaxivity profiles for solutions of ^{14}N-TEMPOL at different temperatures ranging from 25 to 80 °C. Best fit profiles are shown as lines.

the sum of the contributions to relaxation from the translational diffusion of water molecules freely diffusing around the radical, and from water protons bound to the radical at a fixed distance, r, from the paramagnetic center, and in fast exchange with the bulk solvent.

A very good fit was indeed obtained with a unique value of r and of the distance of closest approach, d. The resulting best fit parameters are reported in Table 2. From the standard deviation of the best fit parameters, the error of the correlation time values can be estimated to be between 5 and 10%. Although the effect of possible local motions faster than the global reorientation time of the complex is not taken into account explicitly in the present model, the quality of the fits was very good. Therefore, the inclusion of further parameters related to these fast motions would not permit us to obtain accurate estimates of the fitting parameters due to their large covariance. The contribution from the inner-sphere term amounts to about 30% of the total relaxivity at low fields for the profile at 25 °C. The diffusion coefficient D at 25 °C is in agreement with the expectations and with previous results for the same and similar nitroxide molecules.[12,19,22] It increases with temperature in very good agreement with the T/η dependence (where η is the viscosity). The correlation time in the inner-sphere term results in a smaller value compared to the diffusional correlation time. Since the former is ascribed to the reorientation time of the molecule, this indicates that the paramagnetic molecule rotates significantly in the time it takes for the solvent water molecules to approach the paramagnetic molecule. Furthermore, it should be considered that the unpaired electron is not located at the center of the radical. This causes a rotational contribution to relaxation that is not accounted for by the translational diffusion model. Therefore, the inner-sphere term may not represent a real water molecule actually bound to the radical with a lifetime longer than τ_c, but may simply report such a rotational effect occurring during solvent diffusion. Because of the non-central position of the unpaired electron in the radical, d has a value related to the weighted average of the distances of closest approach for the different directions along which the water molecules approach the radical.[19]

The NMRD coupling factors at 400 MHz proton Larmor frequency have been calculated from the above parameters and the equations are reported in the Experimental section, as a function of temperature, and shown in Fig. 8 (also reported in Table 2). The coupling factor increases by more than a factor of 5 on passing from 25 °C (ξ = 0.008) to 80 °C (ξ = 0.050).

Table 2 Best fit parameters of the field dependent relaxation profiles and corresponding coupling factors at 400 MHz

T (°C)	τ_c (ps)	r (Å)	d (Å)	D (10^{-9} m^2 s^{-1})	τ_D (ps)	ξ_{400} (MHz)
25	17.3	2.78	2.88	2.74	30.3	0.008
35	12.9			3.61	22.3	0.012
45	11.2			4.74	17.5	0.018
55	7.84			5.46	15.2	0.026
62	6.12			5.92	14.0	0.031
72	4.60			6.95	11.9	0.042
80	3.90			7.66	10.8	0.050

Coupling factor ξ from DNP experiments

Having determined the leakage factor (Table 1), the saturation factor (Fig. 6) and the experimental DNP enhancement as a function of temperature (Fig. 3), eqn (1) can now be used to calculate the concentration independent coupling factor ξ from the DNP experiments for the respective sample temperature. This is depicted in Fig. 8 for several experiments and sample sizes, yielding a plot of coupling factor as a function of sample temperature. The figure shows that the data are well reproducible, even for different sample sizes and hence different heating and saturation behaviour, *i.e.* our procedure accurately extracts f, s and the temperature. Referring to biomolecular applications at physiological temperatures (*e.g.* 45 °C), the maximum DNP enhancement will be −14 at full saturation of

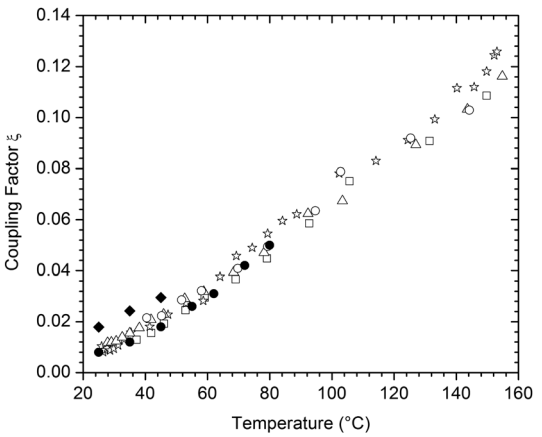

Fig. 8 Coupling factor (enhancement) between the ^{14}N-TEMPOL radicals and the water protons *versus* the sample temperature. The DNP experiments were performed using 30 μm (□,○,△) and 20 μm (☆) ID capillaries. The spread of the experimental data points indicates the statistical errors in enhancement and heating reproducibility. Coupling factors determined through the field dependent relaxation measurements (●) as well as by molecular dynamics[34] (◆) are also shown for comparison.

EPR transition, as calculated from the expected coupling factor of 0.02.

Conclusions

We were able for the first time to determine the saturation factor s of high field DNP measurements, exploiting the paramagnetic shift induced by a high concentration of our polarizing agent (^{14}N-TEMPOL). For a high radical concentration (1 M) full saturation could be achieved already with moderate microwave power (200 mW). We determined the elevated sample temperature under MW irradiation by using an ethylene glycol doped reference sample, which exhibits a temperature dependent relative chemical shift. For high MW power (1 W) surprisingly high temperatures of up to 160 °C could be reached.

With knowledge of the saturation factor s, leakage factor f as well as the sample temperature during the experiment, the coupling factor ξ, which is concentration independent, could be calculated from the experimental data as a function of temperature (Fig. 8).

The value obtained for the coupling factor ξ at 45 °C from the DNP experiments is slightly lower than the value of $\xi = 0.03$ predicted by molecular dynamics simulations (MD) for 9.2 T (260 GHz) at this temperature[35] and it compares rather well to the ξ values predicted from NMR relaxation dispersion curves for this and similar nitroxide radicals in water.[12,19,22,36,37] The increase with temperature is nicely reproduced in both cases (MD and NMRD). Although the possible presence of fast local motions may cause an underestimation of the coupling factor at high magnetic fields, when calculated from the NMRD profiles and analyzed using the hard sphere model,[40] the value derived for the present system at 9.2 T (400 MHz proton Larmor frequency) is rather close to the experimentally observed value.

Alternatively, our experimentally observed DNP enhancement of $\varepsilon = -11$ obtained at 9.2 T and 45 °C can be compared to the experimentally determined DNP enhancements of $\varepsilon = -50$[10] and -63[11] obtained at a somewhat lower magnetic field of 3.4 T (95 GHz/W-band). Taking the theoretically predicted field dependence of $\xi \sim B_0^{-2}$ for rotational motion[18,38] and $\xi \sim B_0^{-3/2}$ (ref. 35 and 39) for translational motion, respectively, these values compare again rather well with our data, taking into account the different experimental setups used and the uncertainties for ε, T and s.

We observe very large integrated enhancements of up to -83 in aqueous solutions of 1 M ^{14}N-TEMPOL at temperatures of about 160 °C. Therefore the very high enhancements observed for TEMPOL and Fremy's salt[14] are partly due to very high temperatures achieved in the tiny sample capillaries by microwave heating. A second effect which may be important in producing higher coupling factors than expected from the magnetic field dependence can be related to additional dynamic modes, which were observed in MD simulations, and in the case of the TEMPOL–water system can be modelled within the classical force-free model[41] by inclusion of fast reorientation times and the associated order parameters.[42] Taking both effects into account permits us to achieve coupling parameters derived from NMRD experiments similar to coupling parameters calculated from MD simulations and in good quantitative agreement with the experimentally observed DNP enhancements at 9.2 T. Despite the fact that the maximum enhancements were obtained for samples with very high radical concentrations (to observe the paramagnetic shift) and very high temperatures (to saturate the electron spin system), reasonable good enhancements of $\varepsilon \approx -14$ can be achieved at 9.2 T magnetic field for a sample with a moderate radical concentration of 20 mM (corresponding to a leakage factor $f = 0.9$) and at a temperature of 45 °C, if full saturation of the electron spin transition is achieved.

Outlook

A new resonator design[40] will render much larger sample volumes, improve the NMR performance (sensitivity and linewidth) and lessen the problem of MW heating. Together with sufficiently large enhancements at high magnetic fields and at ambient temperature this leads the way towards applications of this new approach towards analytics of size restricted samples such as for example biofluids or for biomolecular structural research.

Acknowledgements

This work was supported by the DIP program from the German Research Council (DFG), the Center for Biomolecular Magnetic Resonance Frankfurt (BMRZ), the European Commission, contract Bio-NMR no. 261863, and the COST Action TD1103. We thank Burkhard Endeward, Andriy Marko, Marat Gafurov, Johanna Baldus, Frank Löhr and Christian Richter from the Goethe University for experimental support and Shimon Vega from the Weizmann Institute for stimulating discussions. Also, we gratefully acknowledge technical support from Bernhard Thiem, Manfred Strupf, Bernhard Klug and the mechanical workshop of the Institute of Physical Chemistry in Frankfurt.

References

1 A. W. Overhauser, *Phys. Rev.*, 1953, **92**, 411–415.
2 T. R. Carver and C. P. Slichter, *Phys. Rev.*, 1953, **92**, 212–213.
3 T. R. Carver and C. P. Slichter, *Phys. Rev.*, 1956, **102**, 975–980.
4 L. R. Becerra, G. J. Gerfen, R. J. Temkin, D. J. Singel and R. G. Griffin, *Phys. Rev. Lett.*, 1993, **71**, 3561–3564.
5 J. H. Ardenkjaer-Larsen, B. Fridlund, A. Gram, G. Hansson, L. Hansson, M. H. Lerche, R. Servin, M. Thaning and K. Golman, *Proc. Natl. Acad. Sci. U. S. A.*, 2003, **100**, 10158–10163.
6 K. Golman, R. i. t. Zandt, M. Lerche, R. Pehrson and J. H. Ardenkjaer-Larsen, *Cancer Res.*, 2006, **66**, 10855–10860.
7 C. Song, K.-N. Hu, C.-G. Joo, T. M. Swager and R. G. Griffin, *J. Am. Chem. Soc.*, 2006, **128**, 11385–11390.
8 M. Reese, D. Lennartz, T. Marquardsen, P. Höfer, A. Tavernier, P. Carl, T. Schippmann, M. Bennati,

T. Carlomagno, F. Engelke and C. Griesinger, *Appl. Magn. Reson.*, 2008, **34**, 301–311.
9 S. Hu, M. Zhu, H. A. I. Yoshihara, D. M. Wilson, K. R. Keshari, P. Shin, G. Reed, C. von Morze, R. Bok, P. E. Z. Larson, J. Kurhanewicz and D. B. Vigneron, *Magn. Reson. Imaging*, 2011, **29**, 1035–1040.
10 P. J. M. van Bentum, G. H. A. van der Heijden, J. A. Villanueva-Garibay and A. P. M. Kentgens, *Phys. Chem. Chem. Phys.*, 2011, **13**, 17831–17840.
11 E. V. Kryukov, K. J. Pike, T. K. Y. Tam, M. E. Newton, M. E. Smith and R. Dupree, *Phys. Chem. Chem. Phys.*, 2011, **13**, 4372–4380.
12 P. Höfer, G. Parigi, C. Luchinat, P. Carl, G. Guthausen, M. Reese, T. Carlomagno, C. Griesinger and M. Bennati, *J. Am. Chem. Soc.*, 2008, **130**, 3254–3255.
13 M.-T. Türke, I. Tkach, M. Reese, P. Höfer and M. Bennati, *Phys. Chem. Chem. Phys.*, 2010, **12**, 5893–5901.
14 M. Gafurov, V. Denysenkov, M. Prandolini and T. Prisner, *Appl. Magn. Reson.*, 2012, **43**, 119–128.
15 V. Denysenkov, M. J. Prandolini, M. Gafurov, D. Sezer, B. Endeward and T. F. Prisner, *Phys. Chem. Chem. Phys.*, 2010, **12**, 5786–5790.
16 M. J. Prandolini, V. P. Denysenkov, M. Gafurov, B. Endeward and T. F. Prisner, *J. Am. Chem. Soc.*, 2009, **131**, 6090–6092.
17 M. J. Prandolini, V. P. Denysenkov, M. Gafurov, S. Lyubenova, B. Endeward, M. Bennati and T. F. Prisner, *Appl. Magn. Reson.*, 2008, **34**, 399–407.
18 K. H. Hausser and D. Stehlik, *Adv. Magn. Reson.*, 1968, **3**, 79–139.
19 M. Bennati, C. Luchinat, G. Parigi and M.-T. Türke, *Phys. Chem. Chem. Phys.*, 2010, **12**, 5902–5910.
20 L.-P. Hwang and J. H. Freed, *J. Chem. Phys.*, 1975, **63**, 4017–4025.
21 R. A. Wind and J.-H. Ardenkjaer-Larsen, *J. Magn. Reson.*, 1999, **141**, 347–354.
22 M.-T. Türke, G. Parigi, C. Luchinat and M. Bennati, *Phys. Chem. Chem. Phys.*, 2012, **14**, 502–510.
23 V. P. Denysenkov, M. J. Prandolini, A. Krahn, M. Gafurov, B. Endeward and T. F. Prisner, *Appl. Magn. Reson.*, 2008, **34**, 289–299.
24 M. Rohrer, O. Brügmann, B. Kinzer and T. Prisner, *Appl. Magn. Reson.*, 2001, **21**, 257–274.
25 I. Solomon, *Phys. Rev.*, 1955, **99**, 559–565.
26 I. Bertini, C. Luchinat and G. Parigi, *Adv. Inorg. Chem.*, 2005, **57**, 105–172.
27 I. Bertini, C. Luchinat and G. Parigi, in *Solution NMR of Paramagnetic Molecules*, Elsevier, 2001, vol. 2.
28 R. E. Hoffman, *J. Magn. Reson.*, 2006, **178**, 237–247.
29 A. L. Van Geet, *Anal. Chem.*, 1968, **40**, 2227–2229.
30 M. L. Kaplan, F. A. Bovey and H. N. Cheng, *Anal. Chem.*, 1975, **47**, 1703–1705.
31 C. Ammann, P. Meier and A. Merbach, *J. Magn. Reson.*, 1982, **46**, 319–321.
32 L. J. Briggs, *J. Appl. Phys.*, 1955, **26**, 1001–1003.
33 M.-T. Türke and M. Bennati, *Phys. Chem. Chem. Phys.*, 2011, **13**, 3630–3633.
34 R. A. Wind, H. Lock and M. Mehring, *Chem. Phys. Lett.*, 1987, **141**, 283–288.
35 D. Sezer, M. J. Prandolini and T. F. Prisner, *Phys. Chem. Chem. Phys.*, 2009, **11**, 6626–6637.
36 C. Griesinger, M. Bennati, H. M. Vieth, C. Luchinat, G. Parigi, P. Höfer, F. Engelke, S. J. Glaser, V. Denysenkov and T. F. Prisner, *Prog. Nucl. Magn. Reson. Spectrosc.*, 2012, **64**, 4–28.
37 M. Reese, M.-T. Türke, I. Tkach, G. Parigi, C. Luchinat, T. Marquardsen, A. Tavernier, P. Höfer, F. Engelke, C. Griesinger and M. Bennati, *J. Am. Chem. Soc.*, 2009, **131**, 15086–15087.
38 W. Müller-Warmuth and K. Meise-Gresch, *Adv. Magn. Reson.*, 1983, **11**, 1–45.
39 Y. Ayant, E. Belorizky, J. Aluzon and J. Gallice, *J. Phys.*, 1975, **36**, 991–1004.
40 V. Denysenkov and T. Prisner, *J. Magn. Reson.*, 2012, **217**, 1–5.
41 D. Sezer, *Phys. Chem. Chem. Phys.*, 2013, **15**, 526–540.
42 G. Lipari and A. Szabo, *J. Am. Chem. Soc.*, 1982, **104**, 4546–4559.

